RESEARCH ARTICLE

VOLCANICA

Rapid hazard assessment of volcanic ballistic projectiles using long-exposure photographs: insights from the 2010 eruptions at Tungurahua volcano, Ecuador

Benjamin Bernard*

Instituto Geofísico — Escuela Politécnica Nacional, Ladrón de Guevara E11-253 y Andalucía, 6to piso ed. Ing. Civil, Quito, Ecuador

Abstract

Assessing hazard associated to volcanic ballistic projectiles is essential to limit fatal incidents close to erupting vents. Current state-of-the-art methods using high-speed visual and thermal images and volcanic radars permit to obtain high resolution information during explosive events but are limited to few laboratory volcanoes. Nowadays, long-exposure photographs at erupting volcanoes have become common and can be used to obtain meaningful information. In this paper I present a method to extract volcano-physical data from the projectile parabolic trajectory after adequate scaling and projection. The results, obtained from the analysis of 28 photographs from three eruptive phases at Tungurahua volcano in 2010, allowed to constrain the geometry of the vent (20 m-diameter upper conduit and 70 m-diameter inner crater), the diameter of the ballistic projectiles (up to 4.3 m), their launching angle (50 to 90°), their minimum launching velocity (40 to 145 $m\,s^{-1}$), and their maximum range (up to 1400 m from the vent) for low to moderate explosive activity, outside paroxysms. This turnkey method can help to characterize eruptive dynamics as well as to perform rapid hazard assessment at dangerously explosive erupting volcanoes.

Keywords: `Volcanic ballistic projectile; Long-exposure photography; Tungurahua; Hazard assessment;`

1 Introduction

Ballistic projectiles constitute a major volcanic hazard, being the most common cause of fatal incidents within a 5 km radius of a volcanic vent [Brown et al. 2017]. During the 2014 Mount Ontake eruption, 55 of the 58 fatalities were caused by projectile impacts (Tsunematsu et al. 2016). In Ecuador, two volcanologists from the Instituto Geofísico de la Escuela Politécnica Nacional, Victor Hugo Pérez and Álvaro Sanchez, died from a phreatic explosion in March 12th 1993. This hazard is mainly studied through field work on impact craters and deposits [Alatorre-Ibargüengoitia et al. 2012; Maeno et al. 2013] and/or monitoring (punctual or continuous) at currently active volcanoes [Chouet et al. 1974; Ripepe et al. 1993; Hort and Seyfried 1998; Dubosclard et al. 2003; Andronico et al. 2008; Gouhier and Donnadieu 2011; Taddeucci et al. 2012b; Dürig et al. 2015]. Hazard assessment is generally completed with numerical simulations that require a large number of eruptive source parameters: the projectiles properties (size, density and shape), the atmospheric conditions (temperature and pressure at different altitude, speed of tailwind), the explosion characteristics (launching velocity and angle, extent of reduced drag zone), and the local topography [Mastin 2001]. This information is used to produce deterministic or probabilistic hazard maps [Alatorre-Ibargüengoitia et al. 2016; Biass et al. 2016]. Despite a relatively straightforward approach, ballistic projectile hazard assessment is not systematic, one of the main issue being the acquisition of field data [Taddeucci et al. 2017]. High-speed cameras (visible and infrared) and volcanic radars provide new insights on projectiles and gas escape velocity at the vent as well as in flight dynamics [Gouhier and Donnadieu 2008; Taddeucci et al. 2012a; Bombrun et al. 2015]. Nevertheless most of these studies are realized on a limited number of laboratory volcanoes with mostly low-explosive dynamics. In recent years, long-exposure night photographs at volcanoes have flourished, in particular since the revolution of digital cameras. Long-exposures night photographs can be used to record the trajectories of the incandescent projectiles. In this paper I present a new method to extract physical data on the ballistic projectiles such as minimum launching velocity, maximum launching angle, apparent maximum size and maximum distance reach using the trajectory characteristics. This information is used to perform the first assessment of this hazard at Tungurahua volcano using photographs from the 2010 eruptions. A better knowledge and understanding of how these parameters work together at different volcanoes with diverse eruptive dynamics will

*Corresponding author: bbernard@igepn.edu.ec

greatly improve our hazard assessment approach and ultimately help reduce fatalities at active volcanoes.

2 METHODOLOGY

2.1 Camera settings

Some general rules should be followed in order to record the trajectories of ballistic projectiles. A stable tripod is necessary to avoid vibration during the long-exposure shots. The center of the frame should be set on the vent to avoid border deformations and geometrical complications. The roll of the camera should be null (Figure 2). If the vent is hidden within a crater, the camera tilt and azimuth can be accurately (within 0.5°) set using an inclinometer and a compass (with adequate correction of the magnetic north). Any error in the camera positioning will have an effect on the final calculation depending on the distance between the camera and the vent. The focal length must be chosen in order to: 1) optimize the Ground Sample Distance (GSD: pixel size-equivalent in the target area); 2) include all the ballistic projectiles trajectories; 3) minimize lens distortion (focal length ≥ 50 mm). ISO should be set to the maximum recommended by the manufacturer (depending on the camera model) and focal aperture (F-stop) should be set to the largest (depending on the lens model) in order to enable the visualization of the projectiles incandescence without gaining too much noise nor overexposing the picture. The exposure time must be set in order to record most of the trajectories during a single explosive event which will be typically from 15 s to 60 s. Figure 1 is an example of 30 s-exposure photographs at Tungurahua volcano. Camera settings for this study are included in the Supplementary Material 1.

2.2 Image processing

2.2.1 *Scaling the photograph*

The first step in a photogrammetric study is to correctly scale the images. Even if this step is well known, it is generally not detailed in volcanic ballistic projectile analyses. It is necessary to know the geographic position of the camera (x_1, y_1, z_1) and the vent (x_2, y_2, z_2) to calculate the horizontal (d_H) and vertical (d_V) distances between the camera and the vent (Equation 1 and 2), the straight distance (d_S) camera-vent (Equation 3), and the inclination angle (α) of the camera (Equation 4) (Figure 2). This can be done using GPS coordinates and digital elevation models.

$$d_H = \sqrt{(x_1 - x_2)^2 - (y_1 - y_2)^2} \quad (1)$$

$$d_V = |z_1 - z_2| \quad (2)$$

$$d_S = \sqrt{(d_H^2 + d_V^2)} \quad (3)$$

$$\tan_\alpha = \frac{d_V}{d_H}. \quad (4)$$

The angles of view (β_x and β_y) of the camera are calculated using the sensor characteristics (S_x and S_y) and the focal length (l_F) (Equation 5: same equation using S_y). The straight distance (d_S) is then used to calculate the coverage (c) of the picture at the vent (Equation 6). Finally, dividing the coverage by the number of pixels of the photograph (width w_P and height h_P) we obtain the ground sample distance (GSD) at the vent on a plane perpendicular to the camera's line of sight (Equation 7). If the pixel aspect ratio of the camera is 1, the GSD should be equal horizontally and vertically. Nonetheless I found variations of the pixel aspect ratio from 0.99 to 1.0094 using three different cameras.

$$\tan_{\beta_x} = 2 \times \left(\frac{S_x}{(2 \times l_F)} \right) \quad (5)$$

$$c_x = 2 \times d_S \times \tan\left(\frac{\beta_x}{2} \right) \quad (6)$$

$$GSD_x = \frac{c_x}{w_P}. \quad (7)$$

2.2.2 *Data acquisition*

The GSD is used to set the scale of the picture using ImageJ, a free image processing software developed by Rasband [1997–2016]. The next step is to obtain the precise coordinates of the vent (crater bottom) that should coincide with the site where all the ballistic trajectories converge. Coordinates can be extracted with ImageJ using the point tool. If there is not a direct view inside the crater due to the crater rim, it is necessary to look for the convergence zone of the most vertical trajectories and record the coordinates of the intersection between the vertical trajectories and the crater rim. Then the rim-vent height difference, extracted from the DEM, is subtracted to correct the y coordinates.

Long-exposure night photographs such as that shown in Figure 1 typically have hundreds of projectile trajectories, therefore a selection is required when doing the analysis manually. The main objective of this study is to assess the ballistic projectile hazard. On one hand, assuming that the gas jet is directed mostly vertically (which is adequate for Tungurahua), the launching velocity is theoretically maximum for the most vertical trajectories that reach the highest altitude. On the other hand, based on the same hypothesis, the flattest trajectories allow one to estimate the minimum launching angle with lower launching velocity. In between, intermediate launching velocity and angle will provide the maximum reach. The photograph is a 2D projection of a 3D scene, therefore it is important to choose the trajectories that are close to the plane of projection in order to avoid geometrical errors. It is almost impossible to estimate the angle between the trajectory plane

Figure 1: Explosion at Tungurahua volcano, 31 May 2010 (focal length 250 mm, F/5.3, 30 s, ISO 200). Note the parabolic trajectories followed by the ballistic projectiles, their fragmentation when they hit the ground and the subsequent rolling on the steep slopes of the volcano.

and the photograph plane on a single picture without inducing large errors on the launching velocity and angle estimates [Gaudin et al. 2016]. Nonetheless, using a mostly vertically directed gas jet model and an axisymmetric distribution of the ballistic trajectories, it is reasonable to assume that the most external trajectories on the photograph will be probably on planes almost parallel to the projection plane, although there is no way to assess this uncertainty. This error will affect mostly the launching angle, that will be lower in reality, and, to a lower degree, the maximum height of the projectile, that will be lower in reality if the projectile is moving toward the camera and higher if it is moving away from it. The coordinates of five points from each trajectory are extracted using the point tool on ImageJ. This information is completed with the width of the trajectories, measured with the segment tool, that allows to estimate the apparent maximum diameter of the projectiles [Chouet et al. 1974]. The position of the lowest projectile impact and rolling block can also be extracted from the photograph.

2.2.3 *Data processing*

Chouet et al. [1974] used two synchronized cameras in order to resolve the jet orientation and project the trajectories in a 3-dimensional frame. The problem is that this resolution is feasible only if the vent is close enough to measure angle difference between the two cameras or if the cameras are located far away which is logistically difficult. In order to calculate the ballistic velocities Chouet et al. [1974] use the length of the ballistic traces on very short exposures. In the present study I use the characteristics of the ballistic trajectories and resolve their polynomial equations in order to extract the volcano-physical data. The coordinates of each point are recalculated taking the vent as the origin of the $x-y$ coordinate system. The projectile trajectory coordinates (x_t, y_t) are projected on a vertical plane perpendicular to the line of sight of the camera that pass through the vent in order to correct from the camera tilt using Equations 8 and 9 (Figure 2). The real vent position on the picture is used to correct additional tilt in case the vent was not precisely set to the center of the frame. It is important to note that the error in the projection is directly linked to the angle between the vertical plane and the trajectory plane so the projected

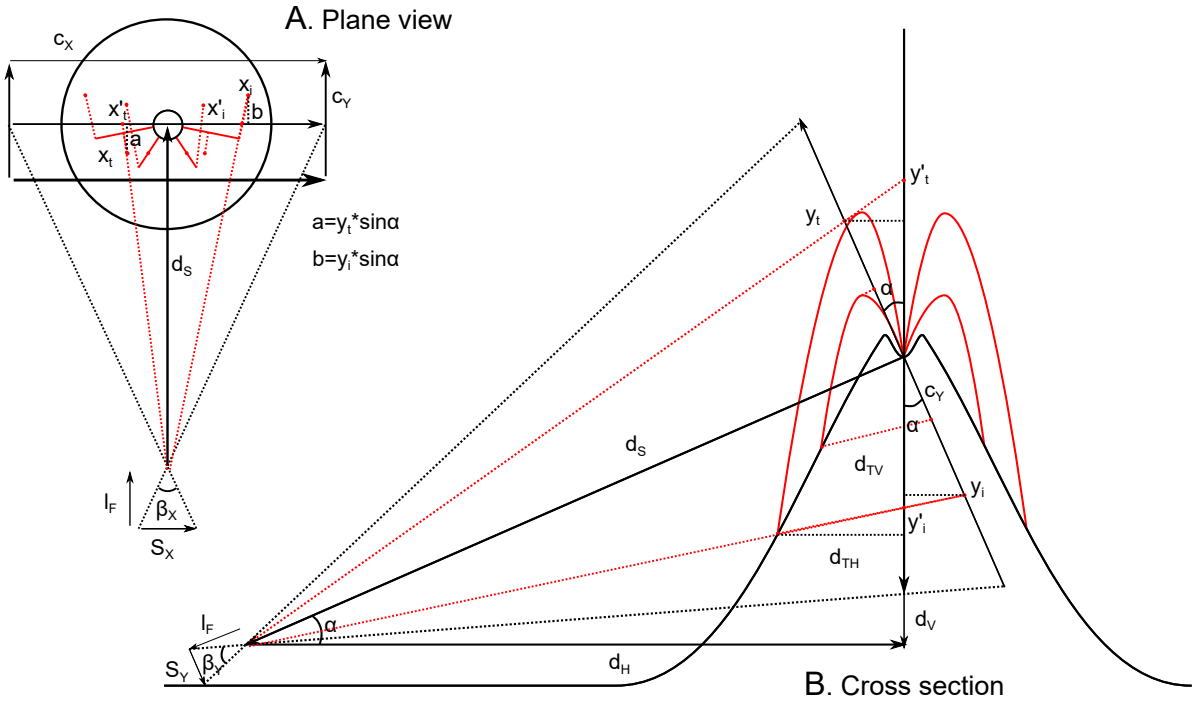

Figure 2: Sketch of the acquisition settings (plane view [A] and cross section [B]) with parameters for the photograph scaling and projection of the trajectory and impact block. Acronyms defined in the text. Note the importance of setting up the most accurately possible the camera position (azimuth and inclination) in order to avoid geometrical errors.

coordinates should be considered as maximum values and the error will be minimized by using the most external trajectories in the picture.

$$x'_t = x_t + \tan\left(\frac{x_t}{d_S}\right) \times y_t \times \sin\alpha \tag{8}$$

$$y'_t = y_t \times \cos\alpha + \tan\left[\alpha + \arctan\left(\frac{y_t}{d_S}\right)\right] \times y_t \times \sin\alpha. \tag{9}$$

The trajectories follow almost perfect second-degree polynomials ($y = ax^2 + bx + c$; Figure 3), so deriving the polynomials at the vent altitude will give the maximum launching angle (MLA) (Equation 10).

$$\tan(MLA) = 2 \times a \times x_{y=0} + b. \tag{10}$$

The top of the ballistic trajectory can be retrieved directly with ImageJ or calculated solving the polynomial equation when the derivative (Equation 10) is equal to 0. The x coordinate at the vent for each trajectory is obtained solving the polynomial equation for $y = 0$, which will have one solution if the trajectory is to the right of the vent on the picture (Equation 11) and a different solution if the trajectory is to the left of the vent on the picture (Equation 12).

$$x_{y=0} = \frac{-b + \sqrt{b^2 - 4ac}}{2a} \tag{11}$$

$$x_{y=0} = \frac{-b - \sqrt{b^2 - 4ac}}{2a}. \tag{12}$$

The maximum height above the vent is used to calculate the minimum launching velocity (mLV) without taking into account the drag that corresponds to a free-fall model (Equation 13).

$$v^2 = 2gh. \tag{13}$$

The trajectory is extrapolated until it intersects the topographic profile parallel to the projection plane in order to obtain the horizontal distance and the altitude that the ballistic projectile should reach without drag (Figure 3). Then the trajectory parameters can be used on any topographic profile to obtain a realistic assessment of the ballistic reach and synthesize it in a hazard map. The projectile impact and rolling block coordinates (x_i, y_i) are projected using Equations 14 and 15 (Figure 2). They are not projected on the volcano topography due to geometrical complications so the values obtained should be considered as maximum for x'_i and minimum for y'_i. As for the projectile trajectories, using projectile impacts close to the edge of the volcano profile will help minimizing this error. The theoretical horizontal distance reached by the block can be estimated using y'_i and topographic profiles.

$$x'_i = x_i + \tan\left(\frac{x_i}{d_S}\right) \times y_t \times \sin\alpha \tag{14}$$

$$y'_i = y_i \times \cos\alpha + \tan\left[\alpha + \arctan\left(\frac{y_i}{d_S}\right)\right] \times y_i \times \sin\alpha. \tag{15}$$

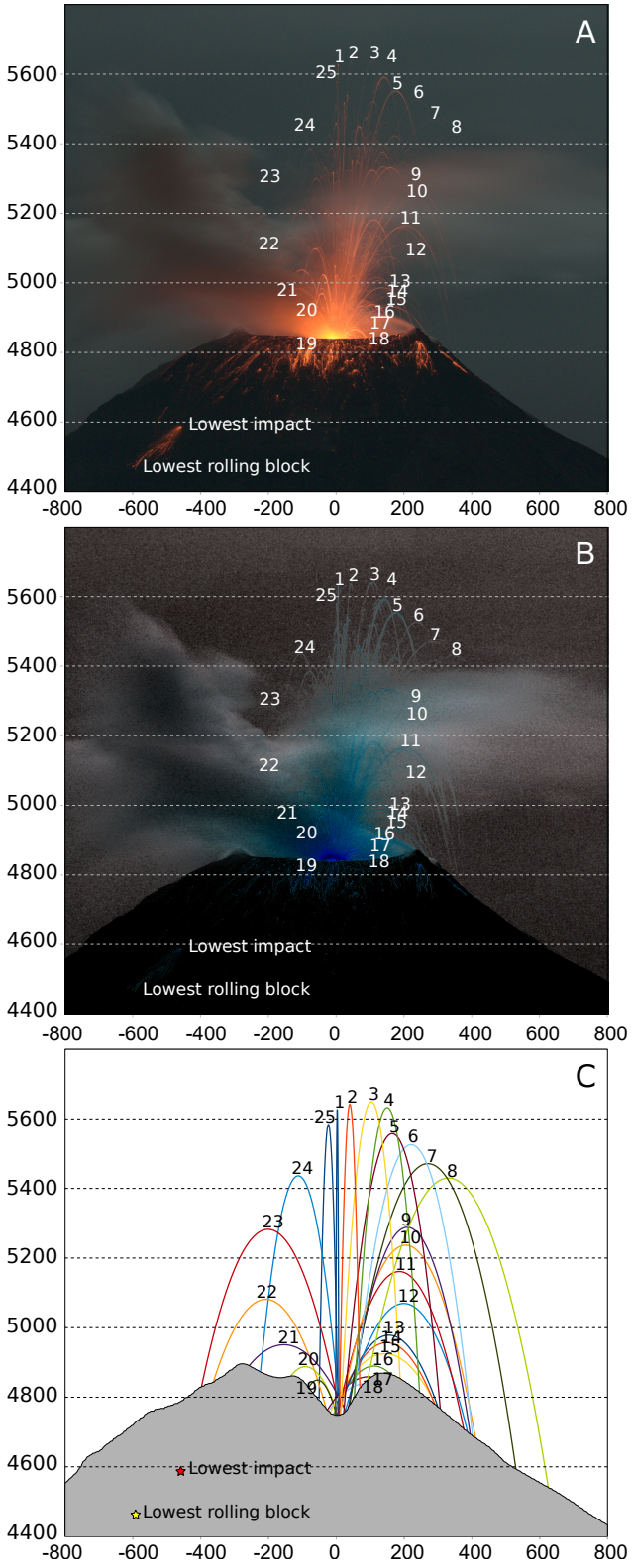

Figure 3: Processing ([A] and [B]) and results [C] of the ballistic trajectory analysis at Tungurahua (picture 2271, 29 May 2010). In order to highlight some trajectories it is possible to invert brightness values or color values [B] in the original picture [A]. Some trajectories like #8 [C] do not appear to come directly from the vent and are possibly associated with near-vent processes such as fragmentation or collisions.

3 Results and Discussion

3.1 Scaling and data acquisition at Tungurahua

In this study, the position of the camera was obtained with a hand GPS (Garmin Oregon 450) with a horizontal precision of ±3 m. The position of the vent was extracted from a 4-m-resolution DEM (source SIGTIER-RAS, published in 2014, images acquired for Tungurahua between 2010 and 2011). Both the camera and the vent heights were extracted from the DEM that has a vertical accuracy estimated at ±1 m. Distances between the camera and the vent can also be extracted from the DEM using a profile tool. Accordingly, the straight distance from the Tungurahua Volcano Observatory to the vent is 13,507 m with an inclination angle of 11.74°. I measured Tungurahua's outer crater width using 5 focal length (120 to 300 mm), with results between 481 and 489 m. It was also measured on the DEM, on a line orthogonal to the camera's line of sight, at 487 m (±4 m), thus supporting the scaling method. On the Tungurahua DEM the crater bottom is ~82 m below the crater rim in the line of sight of the camera so this value is used to correct the vent y coordinate.

In order to test the method I scanned rapidly over 2000 long-exposure night photographs and selected 28 photographs with apparent maximum ballistic height and reach from three eruptive phases from 2010 (January, May–June, and November) that correspond to a total of 8 nights of observations. In January (29, 30) and November (27, 28 and 29), the activity was characterized by an almost constant ash emission with continuous pyroclastic fountaining punctuated by relatively frequent (every 30–60 min) explosions [IGEPN 2018c; IGEPN 2018b]. The May–June activity (29 and 31 May, 03 June) was characterized by more frequent (every 5–10 min) explosions without continuous pyroclastic fountaining [IGEPN 2018a]. Six photographs were used to obtain a large range of minimum launching velocities and maximum launching angle using 15 to 25 trajectories in each photograph (Figure 3). Three of these photographs corresponds to discrete explosions and the others corresponds to continuous pyroclastic fountaining. The rest of the pictures (22) were analyzed for the hazard assessment using between 1 and 4 trajectories for each photograph in order to obtain maximum velocity, maximum trajectory reach, lowest impact and lowest rolling block for each day. The 28 pictures have been processed using ImageJ and a spreadsheet that includes the formulas presented in Image processing but also allows to include the topographic profiles in order to estimate the maximum reach (Supplementary material 2).

3.2 Projectile maximum size, trajectory quality, vent geometry and possible collisions

The size of the projectiles obtained from 157 trajectories was measured between 0.82 and 4.28 m (all results in the Supplementary Material 1). This range is not unexpected as the minimum size would be close to the GSD (about 0.4 m/px in this case). At Tungurahua, videos have shown larger projectiles more than 7 m long. During the 18 October 2013 eruption, a 3-m-wide projectile was found in a PDC deposit [Hall et al. 2015].

The polynomial determination coefficient is extremely good for all the trajectories ($R^2 > 0.96$) with maximum launching angle (MLA) < 85° (Figure 4A). Most vertical trajectories have x coordinates ranges close to the GSD that can produce some error. In general these results confirm that a simple ballistic model that do not take into account atmospheric drag can reproduce the projectile trajectories. Although a free-fall ballistic model is physically wrong and will minimize the launch velocity, it is useful as it will slightly maximize the distance reach, adding an empirical safety buffer, which is adequate in hazard assessment.

The histogram distribution of the horizontal distance between the vent and the trajectories' coordinates at the vent altitude (Figure 4B) gives a good idea about the vent geometry. The median of the distribution is calculated at -1.7 m (1.5 to 4 pixels depending on the focal length) supporting the accuracy of the vent location picking in the photographs even from a distance of about 13.5 km. It is possible to observe a narrow mode that account for ~30% of all trajectories and could correspond to a ~20-m-diameter upper conduit. This estimation is coherent with the 10 m radius observed by Ruiz et al. [2005] and slightly larger than the 3.7–6.7-m-radius calculated by Arellano et al. [2008]. There is also a much wider and flatter mode that accounts for ~60% of all trajectories and could correspond to a ~70-m-diameter source area. According to the 2014 DEM (with images taken between 2010 and 2011) the crater floor in this period was ~43.6 ± 4-m-wide, but the poor resolution and smoothing of the 4-m-resolution DEM can induce some additional error. A recent 5-cm-resolution digital surface model and orthophoto obtained during a drone overflight in January 2018 [Bernard et al. 2018] reveal a 77 × 58-m-diameter inner crater with two sub-circular internal depression (4.8- and 3.1-m-diameter). During the 2010–2016 time span, March 2016 being the last eruptive activity at Tungurahua [Bernard et al. 2017], the vent morphology changed, but according to the three DEM or DSM available taken between 2008 and 2018 the vent location did not moved more than few meters [Bernard et al. 2018] and I presume that the upper conduit diameter did not change significantly. The coherence between the vent geometry extracted from the trajectory analyses and the 2018 drone survey results suggest that complete ballistic trajectories could be as useful as the near-vent straight segments method [Dürig et al. 2015] to reconstruct vent geometry. An advantage of the method presented here is that is also works in case the near-vent straight segments are hidden by the crater rim and can be perform from a much larger and safer distance (13.5 km compared to 850 m in Dürig et al. [2015]. A disadvantage is that it requires information on the crater floor altitude although that can be easily obtained from a DEM.

In the distribution histogram, the outer values (<-30 m and >+40 m) represents only 11.5% of all trajectories and could be associated to trajectories modified by processes such as block fragmentation and collision processes during flight [Vanderkluysen et al. 2012; Tsunematsu et al. 2014; Taddeucci et al. 2017]. This amount of abnormal trajectories is significantly higher than the value obtained by Dürig et al. [2015] for the Eyjafjallajökull 2010 eruption (97 clast-clast collisions over thousands of ejecta) but it is consistent when taking into account the metric-size of the projectiles for Tungurahua's case. Tsunematsu et al. [2014] show that larger particles have higher probability to experience one or more collisions.

3.3 Launching velocity and angle

In general, launching velocities are maximum for the highest trajectories that are also the most vertical ones (Supplementary Material 1). When analyzing the individual datasets (Figure 5A), the range of velocities obtained from the discrete explosion datasets (5197, 2271, 2274) is wider and reach higher values (>130 $m\,s^{-1}$) compared to those from the continuous pyroclastic fountaining ones (5194, 0131, 0132; <100 $m\,s^{-1}$). It is interesting to note that even from a limited dataset our results tend to confirm the observations made on Stromboli on the relationship between height of the ejecta and frequency of explosions [Taddeucci et al. 2013] that are both maximum for the May–June activity and minimum for the January activity. For a given MLA, there is a corresponding maximum mLV that can be reached and it appears a linear relationship between this MLA and the maximum mLV (Figure 5A). The explosion datasets show systematically slopes higher than 1.5 while continuous fountaining have slopes under 1.5. The absence of MLA <50° for the explosions and <60° for the fountaining can be related to the crater rim that hide the lower trajectories. The lowest launching angle is measured in the picture 2271 (29 May 2010) that also accounts for the highest launching velocity. Therefore explosive events with higher velocities are more susceptible to exhibit lower minimum angle if the vent is hidden by the crater rim.

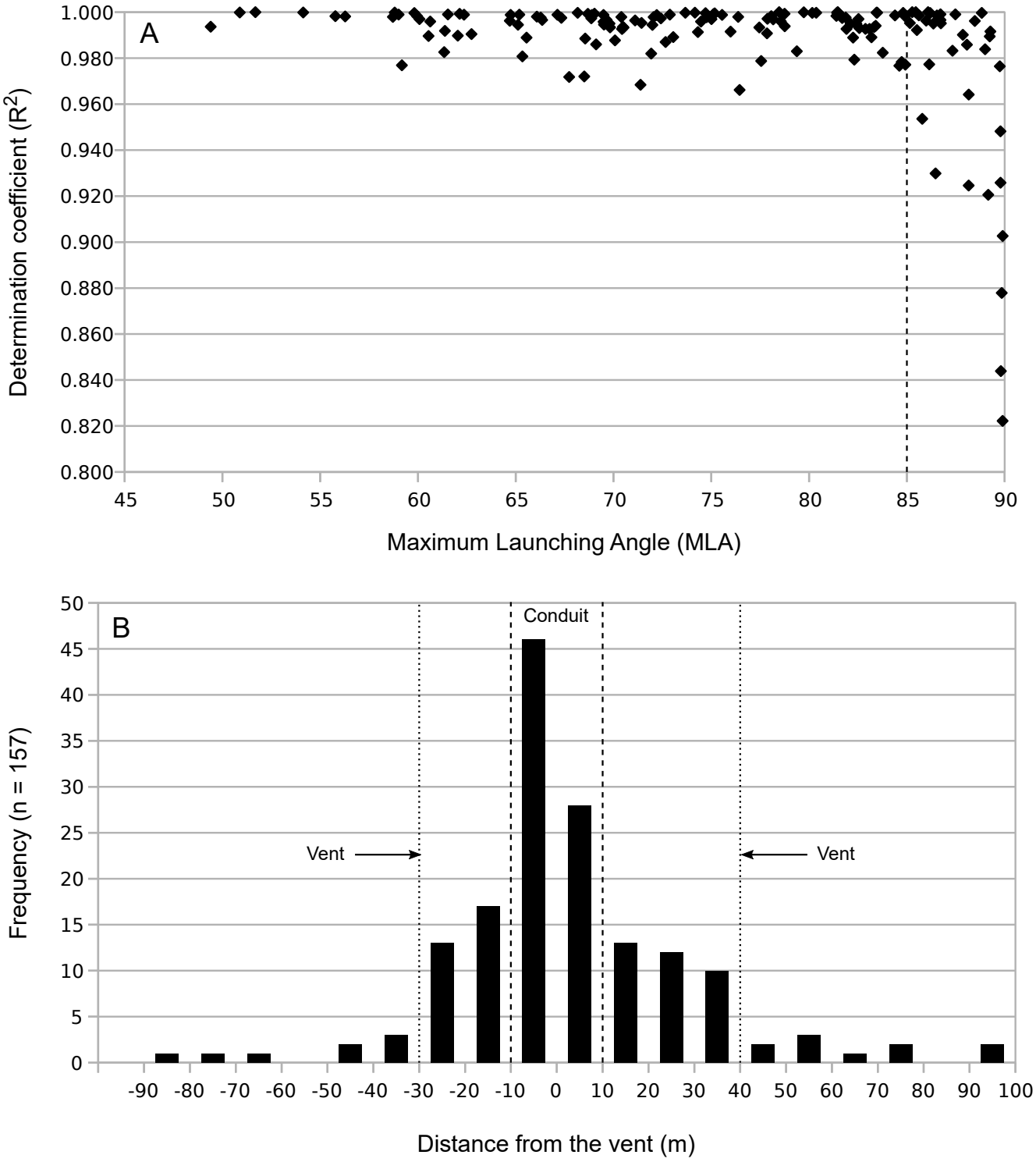

Figure 4: [A] Determination coefficient (R^2) of the polynomial equations compared to the maximum launching angle (MLA) and [B] histogram distribution of the horizontal distance between the vent and the trajectories' coordinates at the vent altitude. Note the excellent R^2 for MLA <85°. Note also the narrow mode between -10 and +10 m, interpreted as the conduit, and wider flatter mode between -30 and +40 m, interpreted as the vent (inner crater).

3.4 Free-fall vs drag modeling

In order to assess the validity of the results presented previously I used the ballistic simulator *Eject!* [Mastin 2001] to include the effect of the drag on the velocity of the ballistic projectiles. I choose two different settings in *Eject!* to reproduce an expected drag scenario (EDS) and a maximum drag scenario (MDS). The EDS includes: variable drag coefficient Cd; a cube shape in aerodynamic position (high); pyroclast density of 1400 kg m^{-3} that corresponds to the average density of 2046 clasts from the 2006, 2013 and 2014 pyroclastic density currents deposits at Tungurahua [García Moreno 2016], and a 100 m zone of reduced drag that corresponds to the superior crater radius. The MDS includes: variable Cd; a cube shape facing the movement direction of the projectile (low); pyroclast density of 640 kg m^{-3} that corresponds to the minimum density in García Moreno [2016]; no reduced drag zone. For both scenarios, thermal lapse rate was set at 6.2 °C km^{-1} and 25 °C at sea level, that is adequate for Ecuador. Block diameter and ejection angle was used according to the trajectory analysis.

The difference between the mLV and the EDS velocity varies from less than 1 % to ~32 % while the difference between the mLV and the MDS velocity varies from ~2 % to ~34.5 %. For launch angles lower than 60° the free-fall model underestimate the projectile initial velocity by about 15 %, and up to 30 % for angles lower than 50°. There is an excellent correlation (R^2 = 0.98) between the maximum launching angle (MLA) and the difference between mLV and EDS velocity (Figure 5B). This correlation is probably due to the difference between the distance traveled by the block in the atmosphere compared to the vertical distance taken into account in the free fall model. For a vertical trajectory the distance traveled by the block to reach its maximum height is close to the maximum height while for an oblique trajectory, the distance traveled by the block to reach its maximum height is much larger than the maximum height. There is more scattering (R^2 = 0.82) when comparing MLA to the difference between mLV and the MDS. This scattering is probably associated with the block diameter variability that will have significantly more influence in the MDS, with the lowest block density, than in the EDS, with an average block density. This might indicate that, as expected, the EDS model is more realistic than the MDS. Both correlations can be used at Tungurahua volcano to make an empirical correction of the mLV based on the MLA to obtain drag model velocities. Using mLV, EDS and MDS velocities allows to have an evaluation of the projectiles' velocity that include a minimum–maximum range.

3.5 Eruptive style and hazard assessment

Eruptive styles at Tungurahua are often characterized as Strombolian, Vulcanian and Sub-Plinian [Eychenne et al. 2013; Hidalgo et al. 2015; Hall et al. 2015]. Comparing with other studies, metric-size ballistic projectiles are not typical of Strombolian and Sub-Plinian activity and are more common during Vulcanian explosions [Maeno et al. 2013; Bombrun et al. 2015; Taddeucci et al. 2017]. Based on the size/velocity inverse relationship [Bombrun et al. 2015], the maximum launching velocities observed for metric-size projectiles at Tungurahua are higher than those expected for Strombolian activity (<100 m s^{-1} for >0.6-m-diameter blocks) with velocities up to 117–135 m s^{-1}, 143–162 m s^{-1} and 144–153 m s^{-1} for January, May–June and November eruptions respectively. The launching velocities are also similar to literature data on Vulcanian eruption (100–400 m s^{-1}) [Druitt et al. 2002; Maeno et al. 2013]. These velocities are significantly lower compared to Sub-Plinian eruptions [Robertson et al. 1998]. In Hidalgo et al. [2015], the January, May–June and November eruptions are named phases IV, V and VI and our photographs fall in the high-explosive activity (HEA) field that is interpreted as Vulcanian activity, supporting the seismo-acoustic analysis from Kim et al. [2014]. Although the Vulcanian classification fit closely the May activity that exhibits discontinuous explosive activity, the January and November activities are characterized by continuous ash venting and pyroclastic fountaining. This activity might be better described as Violent Strombolian eruptive dynamics, also observed at the beginning of Paricutín eruption in 1943 [Blong 1984; Pioli et al. 2008].

In order to compare the apparent reach given by ballistic impacts in the photographs and the theoretical reach obtained extrapolating the ballistic trajectory I projected both on the same topographic profile parallel to the line-of-sight. The maximum theoretical reach for each observation night is in average 30% farther than the maximum apparent reach. This could be explained by an observation bias due to various factors such as the cooling of the projectiles in the atmosphere or because impacts might be hidden by the topography. Also, part of this difference could be attributed to the atmospheric drag. These results show that the external projectile trajectories can be used in order to estimate the maximum reach including a safety buffer. The maximum reach for metric-size projectiles is generally obtained during the Vulcanian explosions (May–June 2010) but there is significant rolling also for periods with mostly Violent Strombolian activity (28 and 29 Nov 2010). This is probably associated with the continuous accumulation of blocks on the high slopes of the cone during the November eruption producing small avalanches driven by gravity. Therefore the rolling blocks should also be considered in the hazard assessment. It is interesting to note that the maximum reach (03 Jun 2010) is not obtained for the photograph with highest launching velocity (29 May 2010), that could be due to either projectile collision or a less-than-vertical directed explosion. It is important to note that none of the obser-

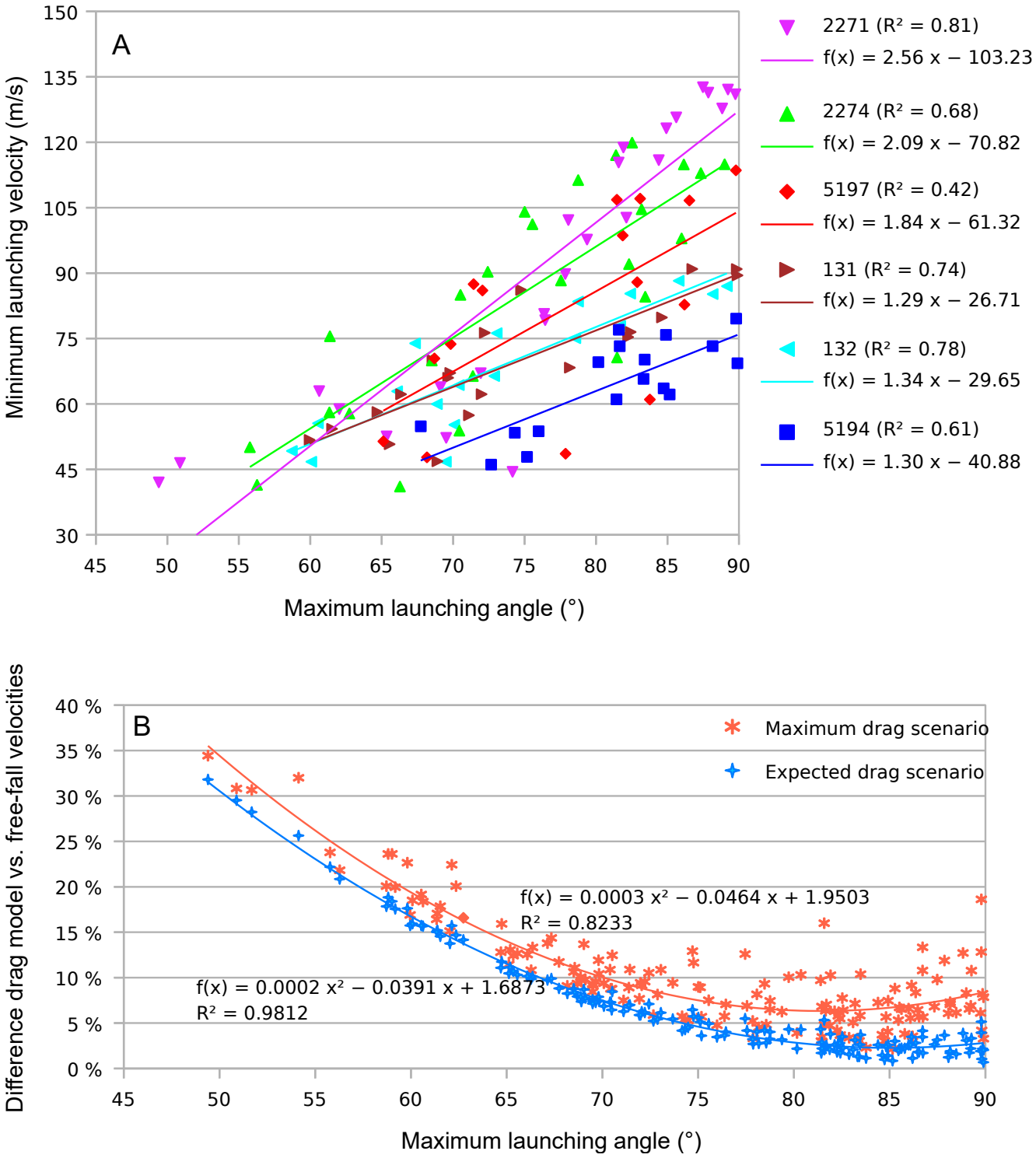

Figure 5: [A] Minimum launching velocity (mLV) compared to maximum launching angle (MLA) for individual datasets and [B] difference between the drag model and the free-fall velocities compared to maximum launching angle (MLA). Note the almost linear relationship between mLV and MLA [A]. Also note the excellent correlation between the difference between the expected drag scenario (EDS) and the free-fall model [B]. The scattering for the maximum drag scenario (MDS) is probably due to the influence of the block size and density.

Table 1 – Maximum values (launching velocity, reach and rolling) from the hazard assessment associated with volcanic ballistic projectiles at Tungurahua in 2010.

	Date							
	29-Jan	30-Jan	29-May	31-May	03-Jun	27-Nov	28-Nov	29-Nov
Minimum launching velocity ($m\,s^{-1}$)	117	101	143	141	135	135	144	133
EDS velocity ($m\,s^{-1}$)	123	103	149	145	141	139	148	137
MDS velocity ($m\,s^{-1}$)	135	107	162	152	152	148	153	147
Theoretical reach (m)	780	244	903	1103	1360	1216	628	911
Apparent reach (m)	375	331	881	785	994	942	427	733
Apparent rolling (m)	449	571	981	872	1278	981	1278	1103

EDS = expected drag scenario; MDS = maximum drag scenario. All values are maxima.

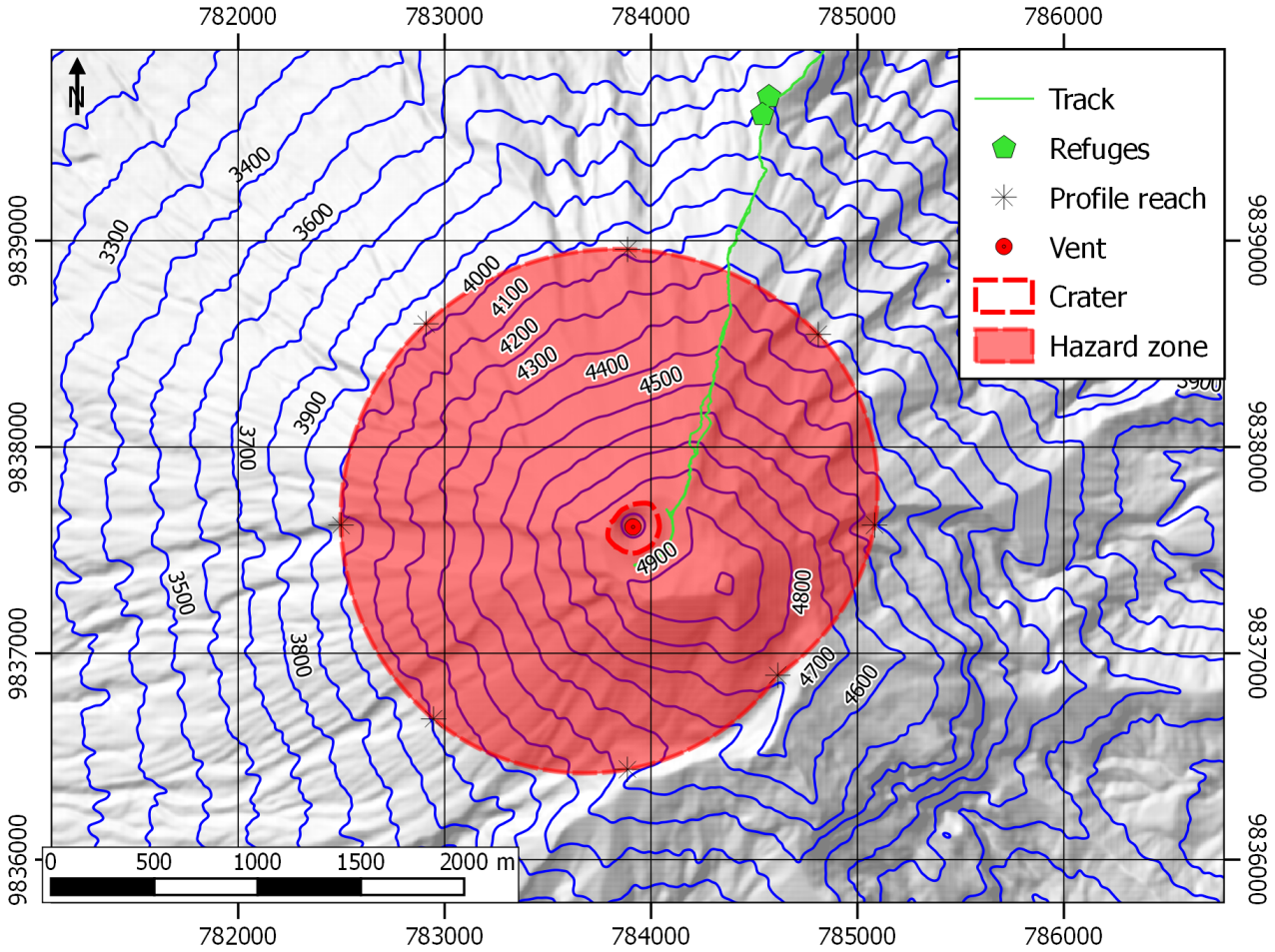

Figure 6: Hazard map for metric-size volcanic ballistic projectiles for low to moderate explosive events (outside paroxysms) at Tungurahua volcano. Coordinates in WGS84 (zone 17 M).

vation nights includes a paroxysm phase so the hazard assessment is only valid for low to moderate but frequent explosive activity at Tungurahua. Using the polynomial equation for the maximum theoretical reach (03 June 2010) and its projection on 8 topographic profiles I present the first ballistic projectile hazard map for such activity at Tungurahua (Figure 6). Depending on the topography metric-size ballistic blocks can reach 1030–1389 m from the crater, the highest reach being in the NW quadrant while the shortest reach is in the SE quadrant. This asymmetry is due to the structure of the volcanic edifice and location of the current vent. Decimetric-size, still potentially lethal, ballistic blocks could have significantly higher initial velocities and higher reach. Nonetheless, it is interesting to note that Tungurahua refuges, located 2 km north of the vent, have been impacted by decimetric-size ballistic projectiles only during Vulcanian and Sub-Plinian paroxysms such as July 14th 2013 and August 16th 2006 eruptions.

4 Concluding remarks

Using trigonometry and long-exposure night photographs it is possible to obtain some relevant volcanological information on the volcanic ballistic projectiles such as size, launching angle and velocity, and reach. At Tungurahua, using 28 photographs from the 2010 eruptions, it is possible to characterize discrete Vulcanian explosions and continuous Violent Strombolian activity. This approach should be applied to other periods of activity at Tungurahua with different eruptive dynamics in order to perform a full hazard assessment. The method presented in this paper can be used as a new monitoring tool for volcanic observatories, even from large distance, knowing the local topography and the camera settings. Even if it has been developed for long-exposure night photography, it can also be used for different set-ups (i.e. videos and thermal imaging). This method can be particularly useful at poorly-accessible and highly-explosive volcanoes, giving the opportunity to perform ballistic projectiles hazard assessment at a significantly larger number of volcanoes without putting scientists in hazardous zones.

Acknowledgements

The author thanks the Instituto Geofísico de la Escuela Politécnica Nacional (IG-EPN) for logistical support during the observation nights at Tungurahua Volcano Observatory. The author thanks the Institut de Recherche pour le développement (IRD) for their financial support of the field work. A special acknowledgment is due to Silvana Hidalgo that reviewed a first version of the manuscript and to Santiago Santamaría that helped with the spreadsheet formulas. This research has been conducted in the context of the Laboratoire Mixte International "Séismes et Volcans dans les Andes du Nord" of IRD. I thank three anonymous reviewers for their constructive comments which helped improving this paper.

Data availability

Raw data (photographs) are available by contacting the author. Supplementary files can be found alongside the online version of this article. Supplementary material 1: Database of Tungurahua VBP; Supplementary material 2: Ballistic calculator spreadsheet; Supplementary material 3: Guideline to use the ballistic calculator.

Copyright notice

References

Alatorre-Ibargüengoitia, M. A., H. Delgado-Granados, and D. B. Dingwell (2012). "Hazard map for volcanic ballistic impacts at Popocatépetl volcano (Mexico)". *Bulletin of Volcanology* 74.9, pp. 2155–2169. doi: 10.1007/s00445-012-0657-2.

Alatorre-Ibargüengoitia, M. A., H. Morales-Iglesias, S. G. Ramos-Hernández, J. Jon-Selvas, and J. M. Jiménez-Aguilar (2016). "Hazard zoning for volcanic ballistic impacts at El Chichón Volcano (Mexico)". *Natural Hazards* 81.3, pp. 1733–1744. doi: 10.1007/s11069-016-2152-0.

Andronico, D., R. Corsaro, A. Cristaldi, and M. Polacci (2008). "Characterizing high energy explosive eruptions at Stromboli volcano using multidisciplinary data: An example from the 9 January 2005 explosion". *Journal of Volcanology and Geothermal Research* 176.4, pp. 541–550. doi: 10.1016/j.jvolgeores.2008.05.011.

Arellano, S., M. Hall, P. Samaniego, J.-L. L. Pennec, A. Ruiz, I. Molina, and H. Yepes (2008). "Degassing patterns of Tungurahua volcano (Ecuador) during the 1999–2006 eruptive period, inferred from remote spectroscopic measurements of SO_2 emissions". *Journal of Volcanology and Geothermal Research* 176.1, pp. 151–162. doi: 10.1016/j.jvolgeores.2008.07.007.

Bernard, B., A. Grouazel, J. Gualpa, M. Almeida, and S. Santamaría (2018). *Volcán Tungurahua: monitoreo térmico y cambios morfoógicos del cráter*. url: http://www.igepn.edu.ec/servicios/noticias/1553-monitoreo-termico-y-cambios-morfologicos-

del-crater-del-volcan-tungurahua-24-01-2018 (visited on 03/20/2018).

Bernard, B. et al. (2017). *Erupción de febrero - marzo 2016 del volcán Tungurahua*. URL: http://www.igepn.edu.ec/servicios/noticias/1463-erupcion-de-febrero-marzo-2016-del-volcan-tungurahua (visited on 03/20/2018).

Biass, S., J.-L. Falcone, C. Bonadonna, F. D. Traglia, M. Pistolesi, M. Rosi, and P. Lestuzzi (2016). "Great Balls of Fire: A probabilistic approach to quantify the hazard related to ballistics — A case study at La Fossa volcano, Vulcano Island, Italy". *Journal of Volcanology and Geothermal Research* 325, pp. 1–14. DOI: 10.1016/j.jvolgeores.2016.06.006.

Blong, R. (1984). *Volcanic Hazards*. 1st ed. New York: Academic Press. ISBN: 9781483288208.

Bombrun, M., A. Harris, L. Gurioli, J. Battaglia, and V. Barra (2015). "Anatomy of a Strombolian eruption: Inferences from particle data recorded with thermal video". *Journal of Geophysical Research: Solid Earth* 120.4, pp. 2367–2387. DOI: 10.1002/2014jb011556.

Brown, S. K., S. F. Jenkins, R. S. J. Sparks, H. Odbert, and M. R. Auker (2017). "Volcanic fatalities database: analysis of volcanic threat with distance and victim classification". *Journal of Applied Volcanology* 6.1. DOI: 10.1186/s13617-017-0067-4.

Chouet, B., N. Hamisevicz, and T. R. McGetchin (1974). "Photoballistics of volcanic jet activity at Stromboli, Italy". *Journal of Geophysical Research* 79.32, pp. 4961–4976. DOI: 10.1029/jb079i032p04961.

Druitt, T. H., S. R. Young, B. Baptie, C. Bonadonna, E. S. Calder, A. B. Clarke, P. D. Cole, C. L. Harford, R. A. Herd, R. Luckett, G. Ryan, and B. Voight (2002). "Episodes of cyclic Vulcanian explosive activity with fountain collapse at Soufrière Hills Volcano, Montserrat". *Geological Society, London, Memoirs* 21.1, pp. 281–306. DOI: 10.1144/gsl.mem.2002.021.01.13.

Dubosclard, G., F. Donnadieu, P. Allard, R. Cordesses, C. Hervier, M. Coltelli, E. Privitera, and J. Kornprobst (2003). "Doppler radar sounding of volcanic eruption dynamics at Mount Etna". *Bulletin of Volcanology* 66.5. DOI: 10.1007/s00445-003-0324-8.

Dürig, T., M. T. Gudmundsson, and P. Dellino (2015). "Reconstruction of the geometry of volcanic vents by trajectory tracking of fast ejecta - the case of the Eyjafjallajökull 2010 eruption (Iceland)". *Earth, Planets and Space* 67.1. DOI: 10.1186/s40623-015-0243-x.

Eychenne, J., J.-L. L. Pennec, P. Ramón, and H. Yepes (2013). "Dynamics of explosive paroxysms at open-vent andesitic systems: High-resolution mass distribution analyses of the 2006 Tungurahua fall deposit (Ecuador)". *Earth and Planetary Science Letters* 361, pp. 343–355. DOI: 10.1016/j.epsl.2012.11.002.

García Moreno, J. (2016). "Mapeo y determinación de parámetros físicos de las corrientes de densidad piroclásticas producidas por el volcán Tungurahua producidas desde el 2006." Engineering thesis. Escuela Politécnica Nacional, Quito, Ecuador.

Gaudin, D., J. Taddeucci, B. F. Houghton, T. R. Orr, D. Andronico, E. D. Bello, U. Kueppers, T. Ricci, and P. Scarlato (2016). "3-D high-speed imaging of volcanic bomb trajectory in basaltic explosive eruptions". *Geochemistry, Geophysics, Geosystems* 17.10, pp. 4268–4275. DOI: 10.1002/2016gc006560.

Gouhier, M. and F. Donnadieu (2008). "Mass estimations of ejecta from Strombolian explosions by inversion of Doppler radar measurements". *Journal of Geophysical Research* 113.B10. DOI: 10.1029/2007jb005383.

– (2011). "Systematic retrieval of ejecta velocities and gas fluxes at Etna volcano using L-Band Doppler radar". *Bulletin of Volcanology* 73.9, pp. 1139–1145. DOI: 10.1007/s00445-011-0500-1.

Hall, M. L., A. L. Steele, B. Bernard, P. A. Mothes, S. X. Vallejo, G. A. Douillet, P. A. Ramón, S. X. Aguaiza, and M. C. Ruiz (2015). "Sequential plug formation, disintegration by Vulcanian explosions, and the generation of granular Pyroclastic Density Currents at Tungurahua volcano (2013–2014), Ecuador". *Journal of Volcanology and Geothermal Research* 306, pp. 90–103. DOI: 10.1016/j.jvolgeores.2015.09.009.

Hidalgo, S., J. Battaglia, S. Arellano, A. Steele, B. Bernard, J. Bourquin, B. Galle, S. Arrais, and F. Vásconez (2015). "SO2 degassing at Tungurahua volcano (Ecuador) between 2007 and 2013: Transition from continuous to episodic activity". *Journal of Volcanology and Geothermal Research* 298, pp. 1–14. DOI: 10.1016/j.jvolgeores.2015.03.022.

Hort, M. and R. Seyfried (1998). "Volcanic eruption velocities measured with a micro radar". *Geophysical Research Letters* 25.1, pp. 113–116. DOI: 10.1029/97gl03482.

IGEPN (2018a). *Informe Especial del volcán Tungurahua No 13*. URL: http://www.igepn.edu.ec/cayambe/868-informe-especial-del-volc%5C%C3%5C%A1n-tungurahua-no-13 (visited on 03/20/2018).

– (2018b). *Informe Especial del volcán Tungurahua No 22*. URL: http://www.igepn.edu.ec/tungurahua-informes/tung-especiales/tung-e-2013/8926-informe-especial-no-22-10octubre/file (visited on 03/20/2018).

– (2018c). *Informe Especial del volcán Tungurahua No 3*. URL: http://www.igepn.edu.ec/tungurahua-informes/tung-especiales/tung-e-2013/8907-informe-especial-no-3pdf/file (visited on 03/20/2018).

Kim, K., J. M. Lees, and M. C. Ruiz (2014). "Source mechanism of Vulcanian eruption at Tungurahua Volcano, Ecuador, derived from seismic moment tensor inversions". *Journal of Geophysical Research: Solid Earth* 119.2, pp. 1145–1164. DOI: 10.1002/2013jb010590.

Maeno, F., S. Nakada, M. Nagai, and T. Kozono (2013). "Ballistic ejecta and eruption condition of the vulcanian explosion of Shinmoedake volcano, Kyushu, Japan on 1 February, 2011". *Earth, Planets and Space* 65.6, pp. 609–621. doi: 10.5047/eps.2013.03.004.

Mastin, L. (2001). "A simple calculator of ballistic trajectories for blocks ejected during volcanic eruptions". *U.S. Geological Survey Open-File Report* 01.45, pp. 01–16.

Pioli, L., E. Erlund, E. Johnson, K. Cashman, P. Wallace, M. Rosi, and H. D. Granados (2008). "Explosive dynamics of violent Strombolian eruptions: The eruption of Parícutin Volcano 1943–1952 (Mexico)". *Earth and Planetary Science Letters* 271.1-4, pp. 359–368. doi: 10.1016/j.epsl.2008.04.026.

Rasband, W. (1997–2016). *ImageJ*. https://imagej.nih.gov/ij//. Bethesda, Maryland, USA.

Ripepe, M., M. Rossi, and G. Saccorotti (1993). "Image processing of explosive activity at Stromboli". *Journal of Volcanology and Geothermal Research* 54.3-4, pp. 335–351. doi: 10.1016/0377-0273(93)90071-x.

Robertson, R., P. Cole, R. S. J. Sparks, C. Harford, A. M. Lejeune, W. J. McGuire, A. D. Miller, M. D. Murphy, G. Norton, N. F. Stevens, and S. R. Young (1998). "The explosive eruption of Soufriere Hills Volcano, Montserrat, West Indies, 17 September, 1996". *Geophysical Research Letters* 25.18, pp. 3429–3432. doi: 10.1029/98gl01442.

Ruiz, M. C., J. M. Lees, and J. B. Johnson (2005). "Source constraints of Tungurahua volcano explosion events". *Bulletin of Volcanology* 68.5, pp. 480–490. doi: 10.1007/s00445-005-0023-8.

Taddeucci, J., M. A. Alatorre-Ibargüengoitia, O. Cruz-Vázquez, E. D. Bello, P. Scarlato, and T. Ricci (2017). "In-flight dynamics of volcanic ballistic projectiles". *Reviews of Geophysics* 55.3, pp. 675–718. doi: 10.1002/2017rg000564.

Taddeucci, J., M. A. Alatorre-Ibargüengoitia, M. Moroni, L. Tornetta, A. Capponi, P. Scarlato, D. B. Dingwell, and D. D. Rita (2012a). "Physical parameterization of Strombolian eruptions via experimentally-validated modeling of high-speed observations". *Geophysical Research Letters* 39.16, n/a–n/a. doi: 10.1029/2012gl052772.

Taddeucci, J., D. M. Palladino, G. Sottili, D. Bernini, D. Andronico, and A. Cristaldi (2013). "Linked frequency and intensity of persistent volcanic activity at Stromboli (Italy)". *Geophysical Research Letters* 40.13, pp. 3384–3388. doi: 10.1002/grl.50652.

Taddeucci, J., P. Scarlato, A. Capponi, E. D. Bello, C. Cimarelli, D. M. Palladino, and U. Kueppers (2012b). "High-speed imaging of Strombolian explosions: The ejection velocity of pyroclasts". *Geophysical Research Letters* 39.2, n/a–n/a. doi: 10.1029/2011gl050404.

Tsunematsu, K., B. Chopard, J.-L. Falcone, and C. Bonadonna (2014). "A numerical model of ballistic transport with collisions in a volcanic setting". *Computers & Geosciences* 63, pp. 62–69. doi: 10.1016/j.cageo.2013.10.016.

Vanderkluysen, L., A. J. L. Harris, K. Kelfoun, C. Bonadonna, and M. Ripepe (2012). "Bombs behaving badly: unexpected trajectories and cooling of volcanic projectiles". *Bulletin of Volcanology* 74.8, pp. 1849–1858. doi: 10.1007/s00445-012-0635-8.